

# Influence of deformation on precipitation process in Mg–15 wt.%Gd alloy

Jakub Čížek <sup>a,\*</sup>, Ivan Procházka <sup>a</sup>, Bohumil Smola <sup>a</sup>, Ivana Stulíková <sup>a</sup>, Vladivoj Očenášek <sup>b</sup>

<sup>a</sup> Faculty of Mathematics and Physics, Charles University, V Holešovičkách 2, CZ-180 00 Prague 8, Czech Republic

<sup>b</sup> Research Institute of Metals, Panenské Břežany 50, CZ-25070 Odolena Voda, Czech Republic

Received 13 February 2006; received in revised form 20 March 2006; accepted 21 March 2006

Available online 5 June 2006

## Abstract

Mg–Gd is a promising light hardenable alloy with a high creep resistance at elevated temperatures. The supersaturated solid solution of Gd in Mg decomposes in a sequence of the following phases:  $\beta''$  ( $D0_{19}$ )  $\rightarrow \beta'$  (c-base centered orthorhombic-c-bco)  $\rightarrow \beta$  (fcc) stable. Formation of the metastable  $\beta'$  phase causes a strong hardening. Dislocations facilitate nucleation of precipitates. Dislocation density is, therefore, an important parameter which influences the precipitation process. This effect was examined in the present work by comparison the decomposition sequences in Mg–15 wt.%Gd alloy cold rolled to various thickness reductions. It was found that precipitation of the  $\beta'$  phase starts at lower temperatures in the cold rolled specimens.

© 2006 Elsevier B.V. All rights reserved.

**Keywords:** Metals; Precipitation; Dislocations and disclinations; Positron spectroscopies

## 1. Introduction

Lightweight Mg-based alloys allow for a significant weight reduction which is important especially in automotive or aeronautical applications. However, use of conventional Mg-based alloys is limited due to a degradation of their mechanical properties at elevated temperatures. Improved mechanical properties even at temperatures above 300 °C were achieved using heavy rare earth metal alloying elements [1]. The Mg–Gd system is one of the candidates for a novel Mg-based light hardenable alloy having a high creep resistance at elevated temperatures. A high ultimate tensile stress at room and elevated temperatures was found in extruded, quenched and age hardened Mg–Gd alloys already 30 years ago [2]. The solubility of Gd in Mg is relatively high but it decreases significantly with decreasing temperature [3]. It enables to achieve a remarkable precipitation hardening during the decomposition of the supersaturated solid solution [4]. Development of microstructure of solution treated Mg–Gd alloys with increasing temperature was investigated in Ref. [5] using electrical resistivity and hardness measurements combined with transmission electron microscopy (TEM). It was found that the  $\alpha'$ -Mg supersaturated solid solution decom-

poses with increasing temperature into the following successive phases:  $\beta''$  ( $D0_{19}$ ) metastable  $\rightarrow \beta'$  (c-bco) metastable  $\rightarrow \beta$  (fcc) stable. Formation of the coherent  $\beta''$  phase leads to a slight increase of hardness, but the peak hardening is caused by precipitation of finely dispersed semicoherent  $\beta'$  phase [5]. Particles of the  $\beta'$  phase were observed in the orientation relationship  $[0\ 0\ 0\ 1]_{Mg} \parallel [0\ 0\ 1]_{c\text{-bco}}$  and  $\{2\bar{1}\bar{1}0\}_{Mg} \parallel \{100\}_{c\text{-bco}}$ . All three possible orientation relationship modes of the  $\beta'$  phase precipitated as plates on the  $\{2\bar{1}\bar{1}0\}_{Mg}$  matrix planes with the same frequency [5]. The plates are coherent with matrix in the  $\{2\bar{1}\bar{1}0\}_{Mg}$  plane, but the coherency is lost on the edges. On the other hand, the particles of the stable  $\beta$  phase are completely incoherent with matrix and cause only a negligible hardening [5].

The precipitation effects are influenced by concentration of nucleation centers and by diffusivity of solutes. An increase in dislocation density leads to an increase of both the parameters and can, therefore, facilitate the precipitation processes. As a consequence, the precipitation sequence can be modified by variation of dislocation density. The effect of preliminary deformation on precipitation process was observed in Mg–Y–Nd–Zr alloy–WE54 [6]. In the present work this effect was examined in binary Mg–Gd alloy which decomposes following similar sequence as WE54 alloy. We compared the precipitation processes in Mg–15.53 wt.%Gd (Mg15Gd) alloy cold rolled to various reduction of thickness (i.e. containing various dislocation densities).

\* Corresponding author. Tel.: +420 221912788; fax: +420 221912567.

E-mail address: jcizek@mbox.troja.mff.cuni.cz (J. Čížek).

Table 1

Results of chemical analysis of studied specimens

Specimen	Gd (%)	Mn (%)	Fe (%)	Zn (%)	Al (%)	Si (%)	Cu (%)	Ni (%)	Mg (%)
Mg	–	0.014	0.020	0.014	0.020	0.014	0.020	0.014	Balance
Mg15Gd	15.53	0.014	0.020	0.014	0.020	0.014	0.020	0.014	Balance

The concentrations are given in wt.%.

The evolution of microstructure with increasing temperature was investigated in particular with respect to variations of defect types and densities. Positron lifetime (PL) spectroscopy was employed for the defect studies. PL spectroscopy has become a valuable tool for investigations of properties of solids [7]. In particular, positron techniques have demonstrated their ability to identify the nature of defects and defect concentrations in various materials [8]. The capability of PL spectroscopy for investigation of precipitation effects in age hardenable alloys was demonstrated many times by Dupasquier et al [9]. In the present work, PL spectroscopy was combined with direct observations of microstructure by transmission electron microscopy (TEM). Temperature changes of mechanical properties, especially the hardening effect, were monitored by microhardness measurements. The isochronal annealing of the studied alloy was performed exactly in the same way as in Ref. [5]. It allows to compare our results directly with electrical resistivity and TEM data obtained in Ref. [5].

## 2. Experimental details

The Mg15Gd alloy specimens were prepared by squeeze casting. Results of chemical analysis of the specimens are shown in Table 1. Note that concentration of impurities and alloying elements is given in the weight percents in the whole paper. The as-cast material was subjected to solution treatment at 500 °C for 6 h finished by quenching into water of room temperature. The specimens were subsequently cold rolled at room temperature to thickness reduction of 8%, 21%, and 29%. After microstructure characterizations of the as-deformed state, the specimens were subjected to step-by-step isochronal annealing with the effective heating rate 1 K/1 min (20 K/20 min up to 300 °C and 40 K/40 min at higher temperatures), i.e. in the same way as in Ref. [5]. The annealing was performed in a silicon oil bath up to 250 °C and in a vertical furnace with protective Ar atmosphere at higher temperatures. Each annealing step was finished by quenching into water of room temperature. Subsequent microstructure investigations were performed at room temperature.

In addition, two reference Mg (99.95%) specimens subjected to various treatments were investigated: (i) a well annealed (280 °C/30 min, slowly cooled down with furnace) sample, and (ii) a sample cold rolled to the thickness reduction of 35%. The results of chemical analysis of the reference Mg are given in Table 1. Note that the reference specimens were prepared from Mg material of the same purity as those used for squeeze casting of Mg15Gd alloy.

A  $^{22}\text{Na}$  positron source with activity of 1.5 MBq sealed between two 2  $\mu\text{m}$  thick mylar foils was used for PL measurements. A fast-fast PL spectrometer

similar to that described in Ref. [10] was employed in the present work. The timing resolution of the spectrometer was 170 ps (FWHM for  $^{22}\text{Na}$ ) at a typical coincidence counting rate of 120 s<sup>-1</sup>. At least  $10^7$  counts were collected in each PL spectrum. Measured PL spectra were decomposed by means of a maximum-likelihood procedure [11]. Microhardness was measured by Vickers method with loading 100 g for 10 s (HV0.1) using LECO micro-tester device.

## 3. Results and discussion

### 3.1. Reference Mg specimens

The lifetimes  $\tau_i$  and the relative intensities  $I_i$  resolved in PL spectra measured on the reference Mg specimens are shown in Table 2. The well annealed Mg specimen exhibits a single component PL spectrum with lifetime  $\tau_B = (224.8 \pm 0.5)$  ps which agrees reasonably with the calculated Mg bulk lifetime of 233 ps, see [12]. Thus, the specimen can be regarded as a “defect-free” material because it exhibits very low density of defects and virtually all positrons annihilate from the free state.

The cold rolled Mg sample exhibits two-component PL spectrum. The shorter component with lifetime  $\tau_1 < \tau_B$  represents a contribution of free positrons, while the longer component with lifetime  $\tau_2$  comes from positrons trapped at dislocations. Indeed, the lifetime  $\tau_2 = (256 \pm 2)$  ps agrees well with the lifetime of positrons trapped at dislocations in Mg [12,13]. Dislocation density  $\rho_D$  in the specimen can be calculated from the two-state simple trapping model (STM) [8]

$$\rho_D = \frac{1}{v_D} \frac{I_2}{I_1} \left( \frac{1}{\tau_B} - \frac{1}{\tau_2} \right), \quad (1)$$

where  $v_D$  denotes the positron trapping coefficient for dislocations in Mg. In the present work we used  $v_D = 1 \times 10^{-4} \text{ m}^2 \text{ s}^{-1}$  determined in Ref. [14]. Using the Eq. (1) one obtains  $\rho_D = (3.6 \pm 0.5) \times 10^{12} \text{ m}^{-2}$  for the cold rolled Mg specimen. In the frame of STM, the quantity

$$\tau_f^{\text{STM}} = \left( \frac{I_1}{\tau_1} + \frac{I_2}{\tau_2} \right)^{-1} \quad (2)$$

Table 2

Experimental lifetimes  $\tau_i$  and corresponding relative intensities  $I_i$  of the exponential components resolved in PL spectra of studied specimens

Specimen	$\tau_1$ (ps)	$I_1$ (%)	$\tau_2$ (ps)	$I_2$ (%)	$\tau_f^{\text{STM}}$ (ps)
Mg well annealed (280 °C/30 min)	$224.8 \pm 0.5$	100	–	–	–
Mg cold rolled ( $e = 35\%$ )	$210 \pm 4$	$60 \pm 3$	$256 \pm 2$	$40 \pm 2$	$226 \pm 1$
Mg15Gd as-quenched	$224.9 \pm 0.5$	100	–	–	–
Mg15Gd cold rolled ( $e = 8\%$ )	$220 \pm 5$	$82 \pm 3$	$255 \pm 2$	$18 \pm 2$	$226 \pm 1$
Mg15Gd cold rolled ( $e = 21\%$ )	$218 \pm 4$	$70 \pm 3$	$256 \pm 2$	$30 \pm 3$	$228 \pm 1$
Mg15Gd cold rolled ( $e = 29\%$ )	$217 \pm 4$	$65 \pm 3$	$255 \pm 2$	$35 \pm 3$	$229 \pm 2$

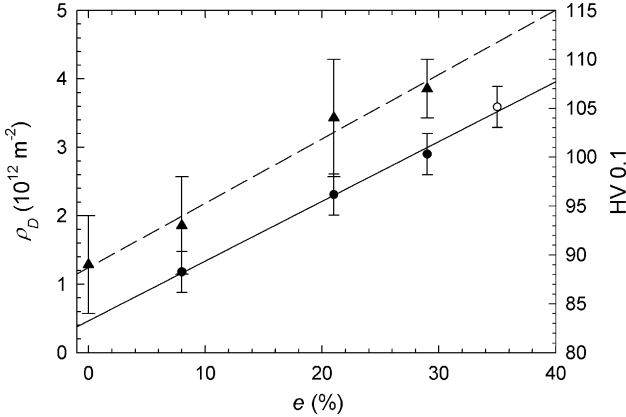


Fig. 1. Dislocation density  $\rho_D$  calculated from Eq. (1) as a function of the thickness reduction  $e$ . Full circles: cold rolled Mg15Gd specimens; open circles: cold rolled Mg. Full triangles (right y-axis): microhardness HV 0.1 measured on the Mg15Gd specimens.

equals to the bulk positron lifetime, i.e.

$$\tau_f^{\text{STM}} = \tau_B. \quad (3)$$

The Eqs. (2) and (3) are often used to check whether the assumptions of the two-state STM (i.e. single type of homogeneously distributed defects, no detrapping) are satisfied. The  $\tau_f^{\text{STM}}$  values calculated from Eq. (2) are shown in the last column of Table 2. Clearly,  $\tau_f^{\text{STM}}$  for the cold rolled Mg specimen agrees well with the Mg bulk positron lifetime.

### 3.2. Mg15Gd specimens

As-quenched Mg15Gd alloy exhibits a single component PL spectrum with lifetime  $\tau_1$  which is virtually the same as that for the well-annealed Mg. Thus, similarly to the well-annealed Mg, the as-quenched Mg15Gd specimen exhibits very low density of defects and can be, therefore, considered as a ‘defect-free’ material. On the other hand, cold rolled Mg15Gd samples exhibit two component PL spectra. The shorter component with lifetime  $\tau_1$  represents a contribution of free positrons, while the longer component with lifetime  $\tau_2$  comes from positrons trapped at dislocations. Dislocation density  $\rho_D$  in the cold rolled Mg15Gd specimens calculated from Eq. (1) is plotted in Fig. 1 as a function of the thickness reduction  $e$ . One can see in the figure that  $\rho_D$  increases approximately linearly with  $e$  as expected for small deformations [15]. Dislocation density in the cold rolled Mg specimen obeys this dependence as well. The  $\tau_f^{\text{STM}}$  values calculated from Eq. (2) for the cold rolled Mg15Gd specimens are slightly higher than  $\tau_B$ , especially for higher deformations. It is most probably due to non-homogeneous spatial distribution of dislocations which is known to result in  $\tau_f^{\text{STM}} > \tau_B$  [16]. Nevertheless,  $\tau_f^{\text{STM}}$  are only a few ps higher than  $\tau_B$ , so that it is still reasonable to use the two-state STM for calculation of dislocation density. Increasing number of dislocations in the cold rolled samples leads to dislocation-induced hardening. It is seen in Fig. 1 as an increase of microhardness with the thickness reduction  $e$ .

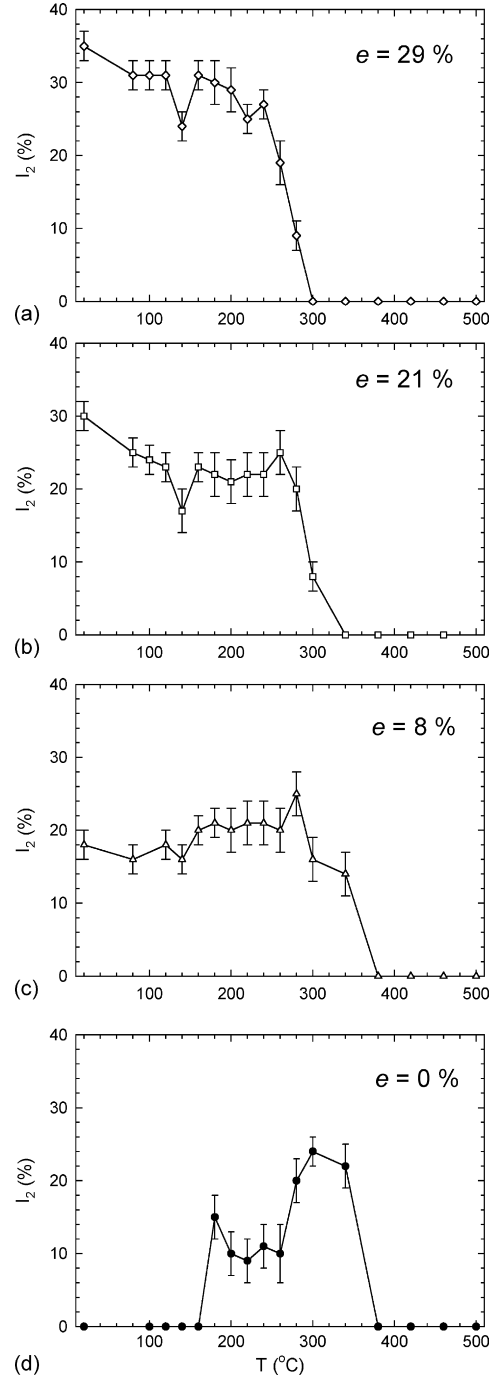


Fig. 2. Temperature dependence of the intensity  $I_2$  of positrons trapped at defects. The lifetime of trapped positrons was fixed to 256 ps, see text for details. (a) Mg15Gd deformed to  $e = 29\%$ , (b) Mg15Gd deformed to  $e = 21\%$ , (c) Mg15Gd deformed to  $e = 8\%$ , (d) non-deformed Mg15Gd.

### 3.3. Precipitation effects in non-deformed Mg15Gd specimens

Misfit defects at the interfaces between the second phase precipitates and the matrix represent trapping sites for positrons. As a consequence, the precipitation effects may lead to an appearance of a defect component in PL spectra. This effect can be seen in Fig. 2d which shows intensity  $I_2$  of the defect compo-

ment for the as-quenched (non-deformed) Mg15Gd specimen as a function of the annealing temperature. The lifetime  $\tau_2$  of positrons trapped at the misfit defects lies very close to that for positrons trapped at dislocations in Mg. In order to reduce the statistical correlation of the fitted parameters, we fixed  $\tau_2$  to 256 ps in the final analysis of the PL spectra. One can see in Fig. 2d that there is no contribution of trapped positrons up to 160 °C in the as-quenched Mg15Gd specimen. At higher temperatures the defect component appeared in the PL spectra. The temperature dependence of microhardness HV0.1 is plotted in Fig. 3d. From comparison of the PL data with HV0.1 and electrical resistivity measured in Ref. [5], one can conclude that the appearance of the defect component with intensity  $I_2$  above 160 °C is due to precipitation of the  $\beta''$  phase. Diffuse spots in electron diffraction pattern demonstrate precipitation of very fine particles of D0<sub>19</sub> hexagonal  $\beta''$  phase after isochronal annealing up to 200 °C. Formation of the  $\beta''$  phase is reflected by a decrease of electrical resistivity [5] and a slight hardening in the temperature interval (180–220) °C, see Fig. 3d. The  $\beta''$  phase particles dissolve with increasing temperature and the c-bcc  $\beta'$  phase is formed in the temperature range (260–340) °C. A bright TEM image of Mg15Gd annealed up to 280 °C is shown in Fig. 4. One can see a high density of finely dispersed  $\beta'$  phase precipitates. The formation of the  $\beta'$  phase leads to a significant drop of electrical resistivity [5] and causes maximum hardening in the specimen, see Fig. 3d. One can see in Fig. 2d that formation of the  $\beta'$  phase causes further increase of the intensity of positrons trapped at defects. Precipitation of the stable  $\beta$  phase in the temperature range (360–420 °C) is demonstrated by a local minimum of electrical resistivity at 420 °C [5]. Very coarse plates (1–2 μm) of the stable  $\beta$  phase were observed in the Mg15Gd specimen annealed up to 420 °C [5]. No hardening caused by formation of the  $\beta$  phase was detected, see Fig. 3d. Similarly, no defect component was observed in PL spectra of the Mg15Gd specimen annealed above 360 °C, see Fig. 2d. It testifies that contrary to the  $\beta''$  and the  $\beta'$  phase, the fraction of positrons trapped at misfit defects at the interfaces of the  $\beta$  phase precipitate–matrix interfaces is negligible. The mean distance between the coarse  $\beta$  phase precipitates becomes too large. As a consequence, the probability of positron trapping in the misfit defects becomes extremely small. No positron trapping at the  $\beta$  phase precipitates was found also in Mg–10 wt.%Gd alloy [12].

#### 3.4. Precipitation effects in cold rolled Mg15Gd specimens

The PL spectra of cold rolled Mg15Gd specimens are well fitted by two exponential components at all the annealing temperatures. Lifetime of positrons trapped at defects remains approximately constant (except of statistical scattering) in the whole temperature range. In order to decrease the statistical uncertainties caused by mutual correlation among the fitted parameters, the lifetime  $\tau_2$  was fixed at 256 ps in the final analysis of PL spectra. The temperature dependence of the intensity  $I_2$  of positrons trapped at defects for cold rolled Mg15Gd specimens is plotted in Fig. 2a–c. Temperature development of microhardness is shown in Fig. 3a–c. The intensity  $I_2$  exhibits a decrease starting from 100 °C in all the cold rolled specimens. It indicates a

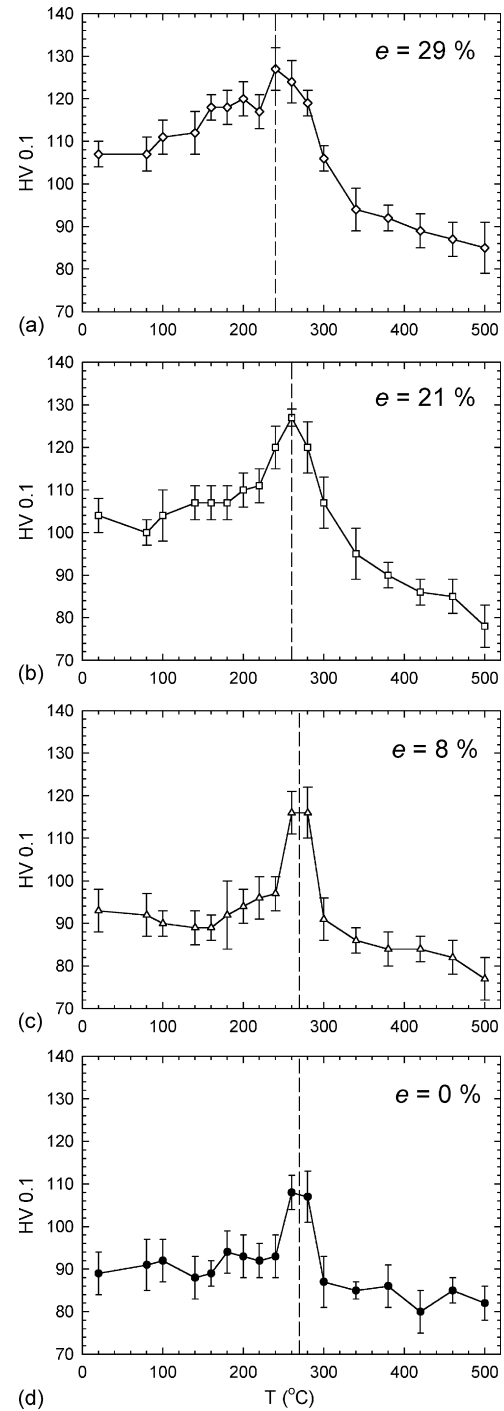


Fig. 3. Temperature dependence of microhardness HV. (a) Mg15Gd deformed to  $e = 29\%$ , (b) Mg15Gd deformed to  $e = 21\%$ , (c) Mg15Gd deformed to  $e = 8\%$ , (d) non-deformed Mg15Gd. The vertical dashed line indicates the peak hardening temperature.

recovery of dislocations. However, this behavior is reversed due to precipitation of the  $\beta''$  phase which leads to an increase of  $I_2$  caused by introduction of misfit defects. The precipitation of the  $\beta''$  phase starts at 160 °C and takes place in the same temperature range as in the non-deformed Mg15Gd. Similarly to the non-deformed specimens, there is only a slight increase of microhardness caused by the precipitation of the  $\beta''$  phase, see

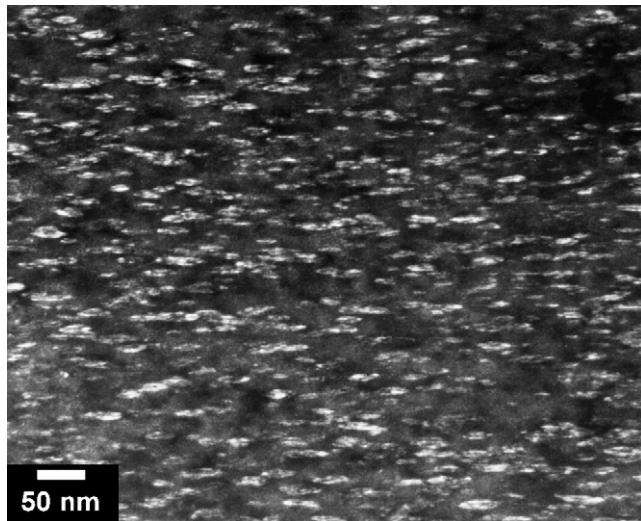


Fig. 4. A dark-field TEM image of non-deformed Mg15Gd specimen annealed up to 280 °C.

**Fig. 3a–c.** On the other hand, formation of the semi-coherent  $\beta'$  phase at higher temperatures causes maximum hardening and an additional increase of  $I_2$ . It is clear from Fig. 3a–d that the maximum of microhardness is shifted to lower temperatures in the cold rolled samples. Formation of the  $\beta'$  phase in the specimens subjected to higher deformation occurs at lower temperatures. It is obviously due to an increase of concentration of nucleation sites by introduction of additional dislocations and enhancement of diffusion of Gd atoms by pipe diffusion. The peak hardness temperature in the specimen cold rolled to  $e=29\%$  is shifted to about of 40 °C lower temperature with respect to the non-deformed specimen. Similarly the strong drop in  $I_2$  caused by growth and dissolution of the  $\beta'$  phase precipitates starts at lower temperatures in the cold rolled specimens, see Fig. 2a–d. Hence, the obtained results indicate that one can change the temperature of maximum hardening in Mg15Gd alloy simply by previous plastic deformation.

#### 4. Conclusions

Thermal development of microstructure and precipitation effects in Mg15Gd alloy were studied by PL spectroscopy combined with TEM and microhardness measurements. It was found that positrons are trapped at vacancy-like misfit

defects at precipitate–matrix interfaces. Precipitation sequences in Mg15Gd specimens cold rolled to various thickness reduction were compared. The investigations revealed that precipitation of the  $\beta''$  phase is not influenced by dislocation density in the specimen. On the other hand, dislocations facilitate nucleation of the  $\beta'$  phase precipitates and formation of the  $\beta'$  phase. As a consequence the peak hardening in cold rolled specimens occurs at remarkably lower temperatures.

#### Acknowledgement

This work was supported by The Czech Science Foundation (contract 106/05/0073).

#### References

- [1] B.L. Mordike, Mater. Sci. Eng. A 324 (2002) 103–112.
- [2] M.E. Drits, Z.A. Sviderskaya, N.I. Nikitina, Technol. Legkikh Splavov 5 (1974) 12–21.
- [3] T.B. Massalski, Binary Alloy Phase Diagrams, 3, 2nd ed., ASM International, Materials Park, OH, 1990.
- [4] S. Kamado, S. Iwasawa, K. Ohuchi, Y. Kojima, R. Ninomiya, J. Japan Inst. Light Met. 42 (1992) 727–735.
- [5] P. Vostrý, B. Smola, I. Stulíková, F. von Buch, B.L. Mordike, Phys. Status Solidi A 175 (1999) 491–500.
- [6] T. Hilditch, J.F. Nie, B.C. Muddle, in: B.L. Mordike, K.U. Kainer (Eds.), Magnesium Alloys and Their Applications, Werkstoff-Informationsges, Frankfurt, 1998, pp. 339–344.
- [7] P. Hautojärvi, A. Vehanen, in: P. Hautojärvi (Ed.), Positrons in Solids. Topics in Current Physics, 12, Springer-Verlag, Berlin, 1979, pp. 1–22.
- [8] P. Hautojärvi, C. Corbel, in: A. Dupasquier, A.P. Mills (Eds.), Proceedings of the International School of Physics “Enrico Fermi”, Course CXXV, IOS Press, Varena, 1995, pp. 491–562.
- [9] A. Dupasquier, G. Kögel, A. Somoza, Acta Mater. 52 (2004) 4707–4726.
- [10] F. Bečvář, J. Čížek, L. Lešták, I. Novotný, I. Procházka, F. Šebesta, Nucl. Instr. Meth. A 443 (2000) 557–577.
- [11] I. Procházka, I. Novotný, F. Bečvář, Mater. Sci. Forum 255–772 (1997) 772–775.
- [12] J. Čížek, I. Procházka, B. Smola, I. Stulíková, Phys. Status Solidi A 203 (2006) 466–477.
- [13] J. Čížek, I. Procházka, B. Smola, I. Stulíková, R. Kužel, Z. Matěj, V. Cherkaska, R.K. Islamgaliev, O.B. Kulyasova, Mater. Sci. Forum 503–504 (2006) 149–153.
- [14] M. Abdelrahman, P. Badawi, Jpn. J. Appl. Phys. 35 (1996) 4728–4729.
- [15] C.H. Reid, A. Gilbert, A.R. Rosenfield, Phil. Magn. 12 (1965) 409–416.
- [16] J. Čížek, I. Procházka, M. Cieslar, R. Kužel, J. Kuriplach, F. Chmelík, I. Stulíková, F. Bečvář, O. Meliknova, R.K. Islamgaliev, Phys. Rev. B 65 (2002) 094106.